BJMHR
British Journal of Medical and Health Research
Journal home page: www.bjmhr.com

Fast Detection of the Angle Between the Hip Bones and Fracture Of Obturator Foramina In Anteroposterior Pelvic X-Ray Based On Mask R-CNN

Kaifeng Liu[1*], Kouki Nagamune[2]
1.Department of Human and Artificial Intelligent Systems, Graduate School of Engineering. University of Fukui
2. Department of Human and Artificial Intelligent Systems, Graduate School of Engineering. University of Fukui

ABSTRACT

A pelvic fracture may lead to multiple complications such as hemorrhage with a high mortality rate. Rapid diagnosis and assessment of injury levels are critical for survival and reduction of morbidity. AP plain x-rays are widely used in the pelvis's rapid evaluation, identification, and primary fixation. In this paper, we retrained the Mask R-CNN model using x-ray images of the pelvis to detect maxillary fractures and measure the angle between the hip bones, which helps classify the trauma mechanism. The method yielded satisfactory experimental results.

Keywords: Multiple sequence alignment, Pairwise sequence identity, Sequence selection treatment, Transmembrane protein, Transmembrane segment

*Corresponding Author Email: liu@u-fukui.ac.jp
Received 05 January 2021, Accepted 22 February 2021

Please cite this article as: Liu K *et al.*, Fast Detection of the Angle Between the Hip Bones and Fracture Of Obturator Foramina In Anteroposterior Pelvic X-Ray Based On Mask R-CNN. British Journal of Medical and Health Research 2021.

INTRODUCTION

The pelvis contributes significantly to protect the internal organs and supporting the weight from the upper body. Its ring structure, which consists of two hip bones and the sacrum as shown in Figure 1, wraps around the intestines and the urinary bladder. As presented in Figure 2, the pubic symphysis forms the connection between the hip bones, works with the ligaments attached to the pelvic surface, such as the iliolumbar ligament, dorsal sacroiliac ligament, anterior sacroiliac ligaments, to maintain the stability of the pelvis. Moreover, as a hub connecting the upper body to the lower extremities, the pelvis has a rich blood supply with well-mixed venous branches and clusters forming around the organs. Consequently, it is highly susceptible to bleeding from exposed fracture sites, soft tissue injuries, and arterial and venous bleeding in low-energy and high-energy injuries. [1]. Among them, low-energy injuries occur mostly in adolescents and the elderly, such as sports injuries in adolescents [2] and damages caused by falls in the elderly [3]. High-energy, such as traffic accident or fall from a significant high, will lead to polytrauma whose Injury Severity Score (ISS) is over 17 points. In addition to injured fractures or bleeding and necrosis of tissues, pelvic bone injuries can lead to functional impairment and failure of uninjured organs and systems [4]. Joerg h. Holstein et al. conducted a study of 5,340 patient records with pelvic bone injuries collected by the German Pelvic Trauma Registry from April 30, 2004, to July 29, 2011. They found that 27% of the deaths were due to pelvic injury, with pelvic hemorrhage being the leading cause. Among these patients, 39% died within the first 24 hours, while 53% died within 48 hours [5]. Additionally, multiple blunt trauma is also a significant cause of pelvic bone injury, leading to embolism and death [6]. Rapid and accurate diagnosis, reasonable first aid procedures, and effective treatment plans are the critical factors for improving survival rate, reducing morbidity, and improving outcomes.

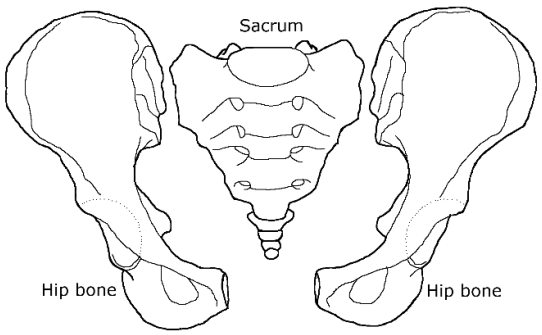

Figure 1: Structure of pelvic

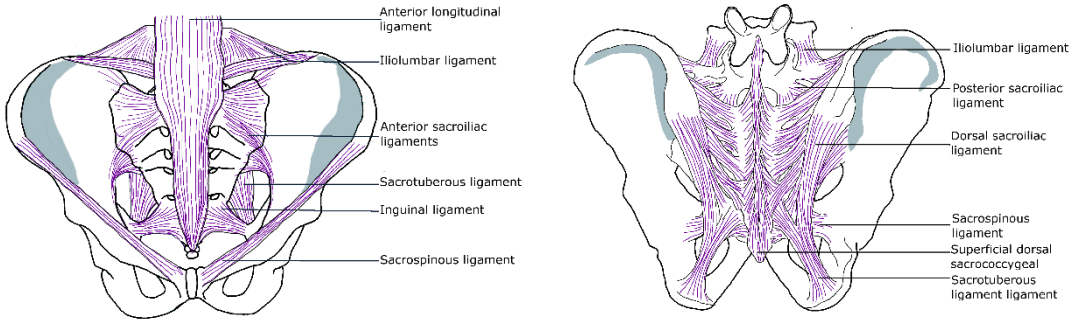

a. anterior aspect b. posterior aspect

Figure 2: Ligaments on pelvis

X-ray radiography and computed tomography (CT) are commonly used as essential imaging tools for the primary survey of patients with trauma. Despite more injury details that can be provided when the surgeon suing the 3D models built by CT imaging, the extra ionizing radiation released by CT is significantly higher than the traditional radiograph, increasing the risk of other diseases [7]. In contrast, the traditional Plain x-rays, especially the anteroposterior x-ray, have a small amount of radiation and take shorter to perform, which are more sensitive in diagnosing hemodynamic instability and anterior injuries [8, 9]. Due to the advantages of the x-ray we stated above and the need for accurate diagnosis within shot time after trauma, the rapid identification of pelvic damage has considerably attracted a large amount of attention.

In recent years, the algorithm based on convolutional neural networks (CNN) has made significant progress in applying computer vision. Promising results have also been achieved in automatic medical diagnoses, such as detecting pulmonary nodules in the 3D chest CT scan, detecting retinopathy in diabetic patients, and segmentation of 3D knee cartilage [17, 18, 19].

In this paper, we proposed a method of adapting Mask R-CNN for automatic pelvis segmentation. Fit the two hips' centerline and calculate the centerline angle for the identified hips by refinement and other operations. By this method, the angle of the hip bone in a healthy pelvis is measured. For the identified obturator foramina, structural integrity is judged and then provides a basis for determining the type of pelvic injury.

METHOD AND DATASET

Dataset collection

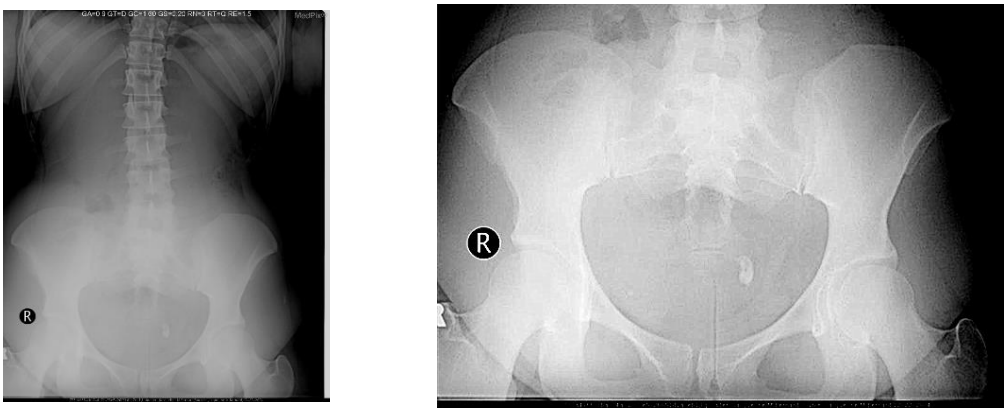

a. The original Image b. The preprocessed image

Figure 3: Image preprocessing

We prepared 160 anterior/posterior (AP) x-ray images for the train set, containing 100 healthy pelvic images and 60 damaged pelvic images, respectively. 50 AP x-ray images for validation set) and 100 AP x-ray images for the test set. All these images are collected from MedPix® and DICOM library. MedPix® is a free open-access online database providing various medical data, such as medical images, medical cases of illness, and integrating images for learning and research [15]. Each image has a detailed pathology introduction to help researchers locate the damaged area quickly and accurately. DICOM library is a free online medical DICOM image or video file sharing service for educational and scientific purposes [16]. Researchers can upload their own Dicom medical image files or view shared images.

Preprocessing was performed on each image we obtained from the open-access online database to remove information other than bone and injure interest in the image. As shown in Figure 3a., some graphics contain annotation information, which is unhelpful to extract location information damage of hipbones and affect the model training in the next step. Then we used computer image processing technology to remove this information. Figure 3b. shows the result after pretreatment.

Mechanism of injury classification

Table 1: Young-Burgess classification

Category of fracture	**Type**		
	I	**II**	**III**
Anterior posterior compression (APC)	Widening of symphyseal is less than 2.5cm without disruption of anterior and posterior ligaments	Widening of the symphysis pubis with anterior ligaments disrupted.	Complete posterior ligamentous and Symphyseal disruption without vertical displacement and sacroiliac joint completely separated
Lateral compression (LC)	Fracture of pubic rami	Contains crescent (iliac wing) fracture	Contains contralateral anterior posterior compression injury
Vertical shear (VS)	Complete ligamentous injury with vertical displacement		
Combined	Contains two or more		

mechanical injuries (CMI)	types of injure at the same time		

Accurate classification of pelvic injury mechanisms and rapid determination of the injury site are prerequisites for a reasonable treatment plan. Young-Burgess classification is widely used in the clinic to predict the extent of the damage done to the pelvis's tissues, organs, and bones [20, 21]. Depending on the external force causing the damage, the Yong-Burgess classification can be divided into four categories which listed in Table 1.

According to the categories' characteristics, APC III and VS are completely unstable, and other categories are partially stable. Rotation and displacement of hipbones and fracture of pubic rami are two essential criteria to classify the pelvic fracture. Figure 4a. shows a healthy human pelvis. When the pelvis is subjected to a large amount of impact energy causing rotation or displacement of the hip bone, the hip bone centerline angle changes significantly (Figure 4b., Figure 4c.). Accordingly, in Figure 4-d the angle of the hipbones and the obturator foramen integrity test can provide a basis for rapid pelvic injury classification. At this point, an AP x-ray has an essential role in the diagnosis of pelvic bone injuries.

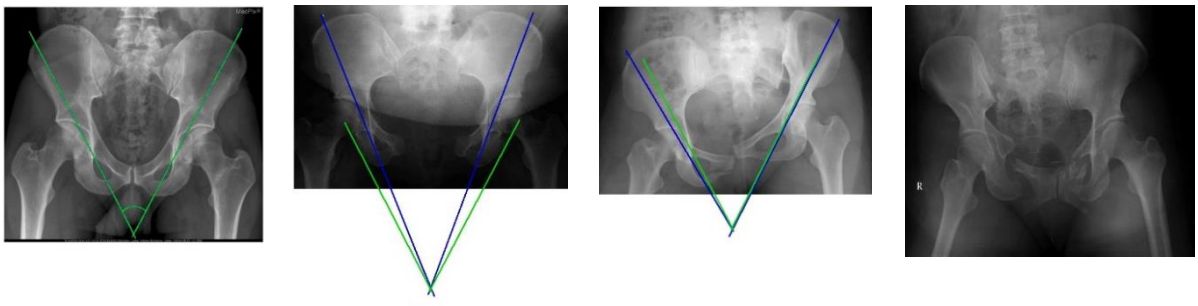

a. Healthy pelvic ring **b. The angle between hipbone is less than normal** **c. The angle between hipbone is larger than normal** **d. Displaced pubic rami fracture**

Figure 4. Ap x-ray can provide a basis for the classification of fracture types

The Mask R-CNN Model

He et al. proposed the Mask-RCNN network structure in 2017, extending the Faster R-CNN to perform pixel segmentation. [22]. Compared with the Fast R-CNN, the Mask R-CNN adds a mask prediction branch to the original architecture. As presented in Figure 5, we can perform object detection and instance segmentation at the same time was benefitting from the parallel processing method. The author replaced the Region of Interest-Pooling (ROI-Pooling) layer with the ROI-Align layer, which uses bilinear interpolation to solve the problem of inaccurate mask generation due to missing edge pixels. Besides, the framework independently predicts a binary mask for each category without introducing inter-class competition, and each binary mask category relies on the classification prediction results given by the network ROI classification branch. During the training phase, a multitasking loss function was defined as

$$L = L_{cls} + L_{box} + L_{mask} \quad (1)$$

For each sampled ROI. Furthermore, the network is highly portable and has achieved the best results in COCO's list of challenging tasks, including segmentation, bounding-box object detection, and crucial human detection. Therefore, applying this framework to medical image segmentation holds significant promising aspects.

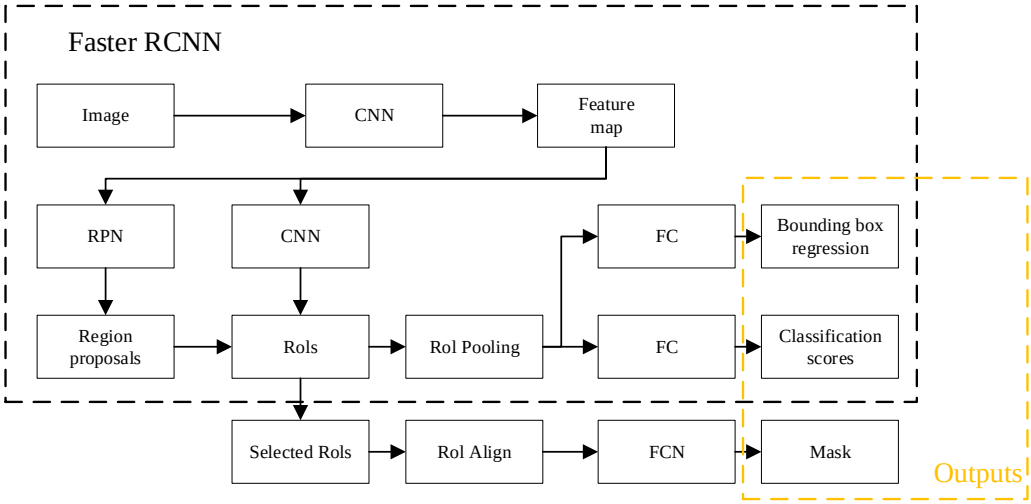

Figure 5: The network architecture of Mask R-CNN used in this research to classification and segmentation

SEGMENTATION AND RECOGNITION

Because of the small number of images in the collected dataset, over fitting occurs quickly and does not provide the expected results if the dataset is used directly in the model. We use our dataset to transfer train a pre-trained model to obtain a new model for pelvic x-ray segmentation, rather than retraining the model with a small amount of data. This pre-trained model is provided by an open-source project conducted by Matterport Inc and running under the MIT License. Matterport Mask R-CNN was pretrained based on the MSCOCO dataset [23], which contains 80 classes covering common animals, plants, and objects in life, making it easy to extend.

The first step of retraining is to annotate the area of hipbones and obturator foramen manually owing to the images collected from shared resources, lack information of ROI. For this experiment, we used Labelme [24], a graphical image annotation tool, to manually label images. Unlike natural Images, x-ray images are generated by sensing photons that are not absorbed by anatomical structures and lack depth information. Some areas of bones overlap in the x-ray image, which reduces the accuracy of instant segmentation. Accordingly, we created two datasets for comparative experiments. One is annotating hipbones and obturator foramina separately, and the other is annotating them in one graph at the same time.

Although we used the weights of the pre-trained Matterport Mask R-CNN model to reduce the training dataset requirements, the size of the dataset used in the processing of transform

training affects the segmentation results, we enhanced the labeled dataset. Considering this stage's aim is the training model for segmentation of the pelvis, we adopted compelling and accessible enhancement techniques, such as flip, rotation, scale, crop, and translation, proven to achieve satisfactory result. Then, JSON files generated by Labelme were converted to MSCOCO data format, which the pre-trained model accepts.

The same training environment as Matterport Mask R-CNN, such as Python, Keras, and TensorFlow library, are used in this experiment. After comparing the results of two groups as the backbone in small-scale training, one is Resnet-50 combined with Feature Pyramid Networks (FPN) [25], and another is Resnet-101 combined with FPN, we chose the second group as the backbone since it can provide better results and the pressure on the hardware during training is negligible. We divided the training into two stages. In the first phase, we only trained the head branch to avoid damaging the base layer's extraction ability. In the second stage, we trained all the layers using the weight of MSCOCO. To keep the training process stable, we used two GPUs for training, and two images per GPU, so that the batch size is 4. Then we used the same configuration and the new model we obtained to segment the pelvis.

We used the obturator foramen's information as the output of the segmentation model to determine whether the pelvic fracture was an anterior fracture of pubic rami. For the mask of hipbones, we performed the image processing method, distance transformation, to obtain the points farthest from the background. Following obtaining the skeleton of the mask in Figure 6, the black curve is the skeleton of the mask of the hipbone, which we cannot use to fit into a straight line directly since people of different genders, ages, or countries may have different degrees of curvature of their hip bones. Crucially, patients with pelvic fractures may be accompanied by pubis, ischial or iliac injuries, which may affect mask skeleton extraction accuracy. To solve this problem, we removed the curved parts at the mask skeleton's ends and kept only the skeleton in the middle of the mask near the rectangular region.

Then, a straight line is fitted to the remaining points using the least-squares method, and the angle between the two lines is calculated based on the slope of the fitted line.

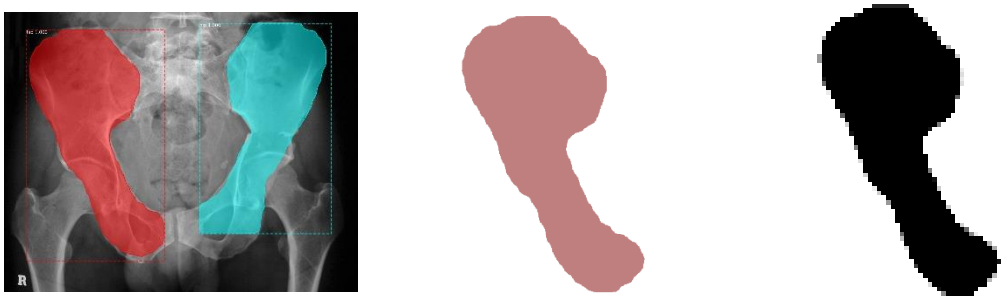

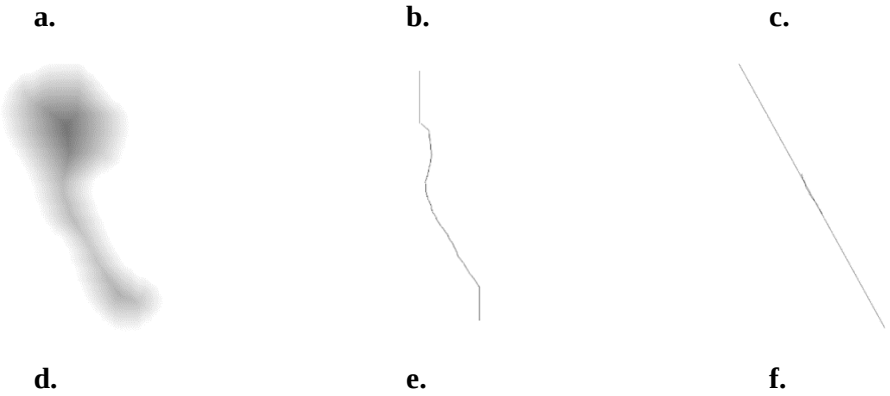

Figure. 6: The processing of fitting lines of hipbones using the masks generated by the model retrained

RESULTS AND DISCUSSION

Figure 7, Figure 8, and Figure 9 show the training loss of the three models. We trained each model for 30 epochs. Although the loss of the verification set rises locally in the training process, the over fitting is limited.

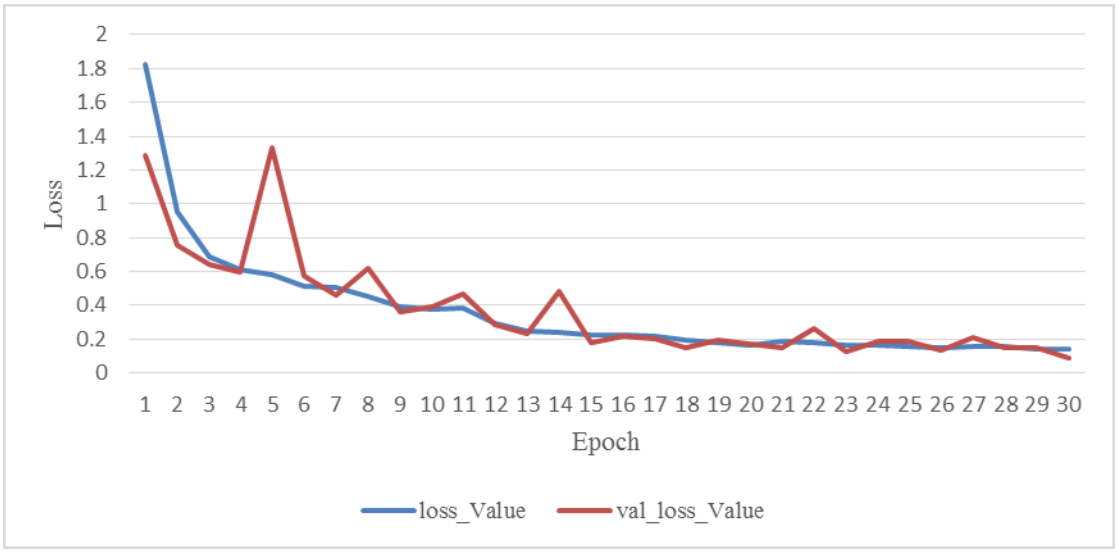

Figure 7: Training Loss of hybrid model

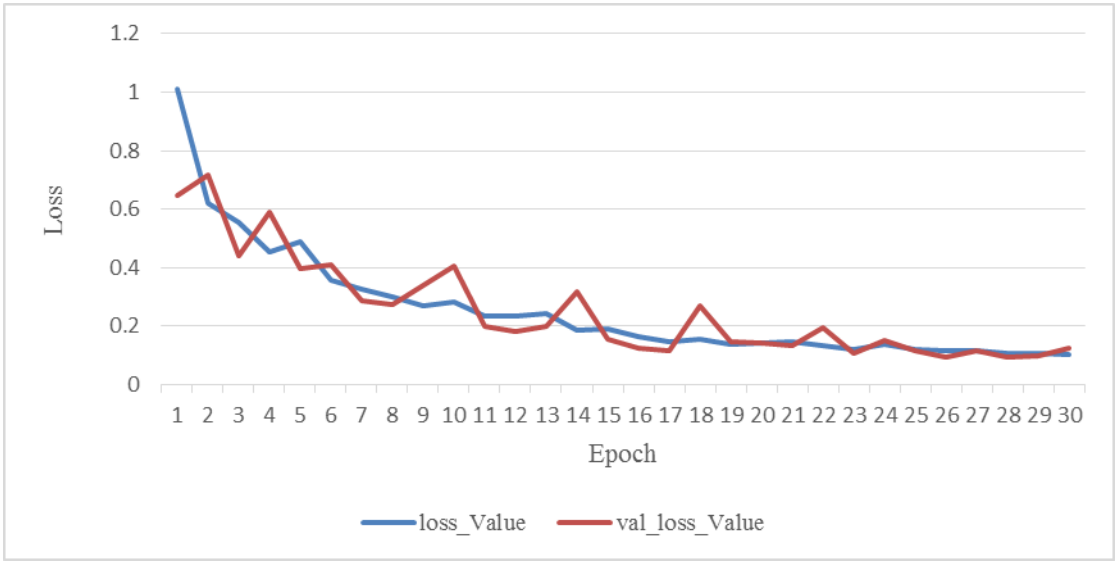

Figure 8: Training Loss of hipbone model

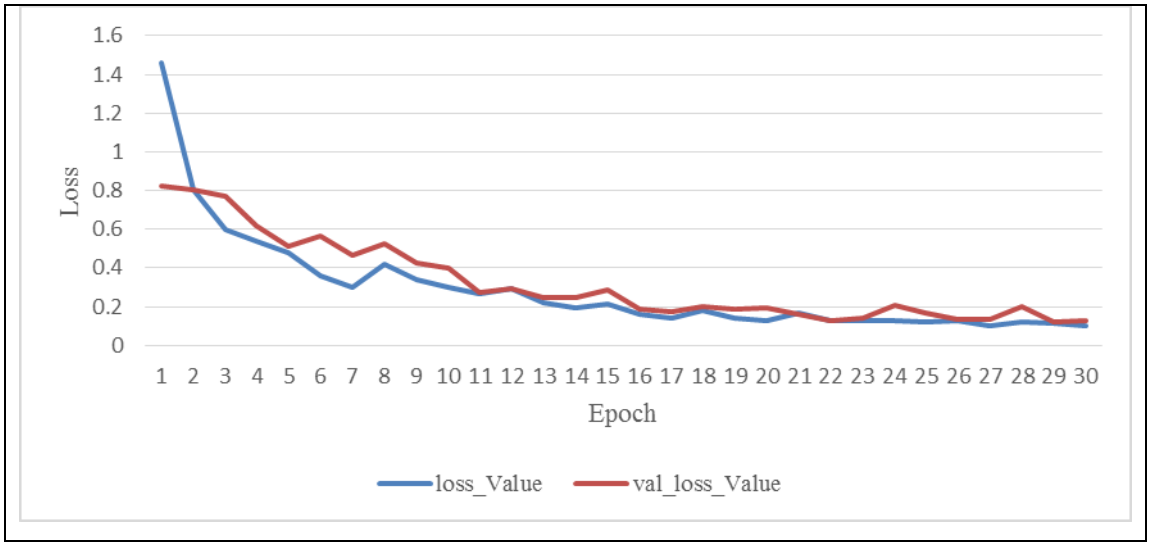

Figure 9:Training Loss of obturator foramen model

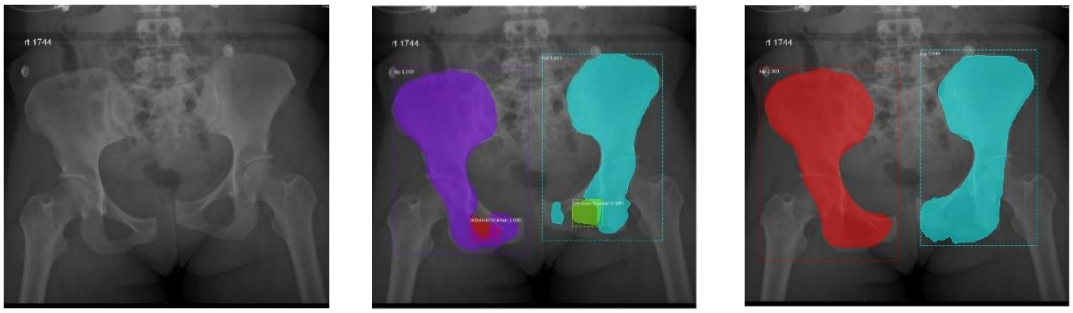

a. The original X-ray **b. The result of hybrid model** **c. The result of hipbone model**

Figure 10. Comparison of experimental results

We compared the segmentation results of the two experiments. One is the hybrid model can segment the hipbones and obturator foamen at the same time. The other is the one that can only provide the mask of hipbones. Figure 10 shows the segmentation results of one image using the two models. Due to the overlap of two objects, the masks interact with each other in production, causing the tearing of the mask and incomplete segmentation. Nevertheless, we can get better results to set hipbones as the only object.

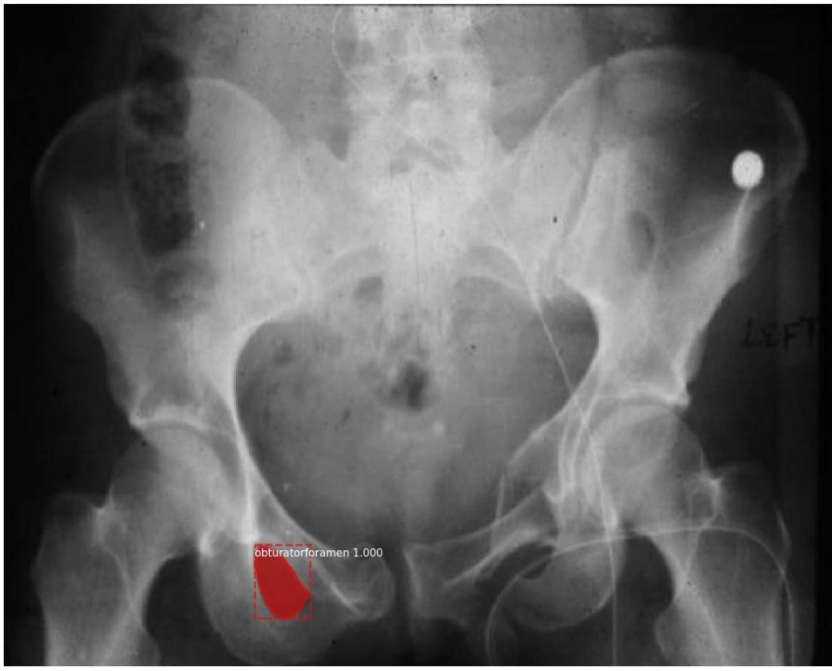

Figure 11. Segmentation of obturator foramen

The model trained for obturator foramen segmentation can recognize intact areas without damage that is there are no superior ramus fractures and displacement. Otherwise, the obturator foramina cannot be recognized and segmented. Figure 11 shows the displaced fracture of the left ramus. Compared with the right side, the left obturator's integrity is damaged and cannot be recognized. 100 X-ray films are divided into two groups as testing data. One group contains 50 films, including healthy pubic rami and pubic rami fracture without displacement, and the other one is 50 films with displaced pubic rami fracture. The results are shown in Table 2, which total discriminant accuracy is 93%. In the four failure instances, one of them identify the shadow in other positions as obturator foremen, and in the other three films, the obturator foramen was damaged and could not be recognized. In the second group, three images are incorrectly identified. In all of them, obturator foramen was incorrectly identified.

Table. 2 Identification results

Types	**Films with ramus fractures**	**Films without ramus fractures**
Number of X-ray	50	50
Correct identification	46	47
Accuracy rate	92%	94%

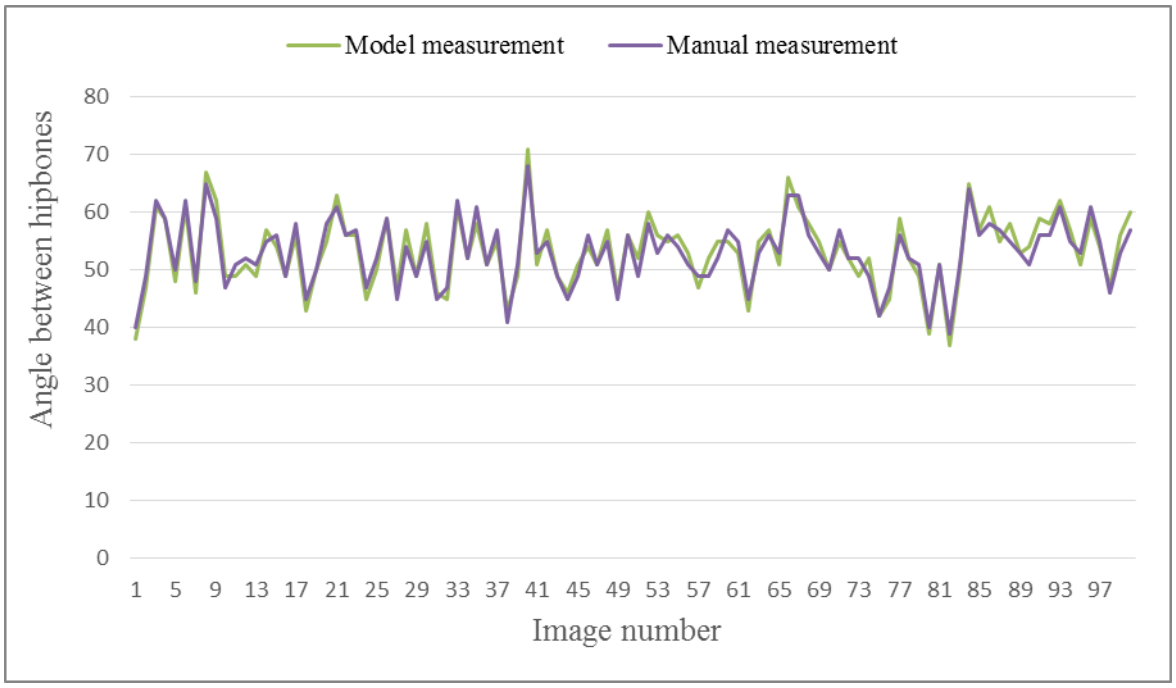

Figure 12: Comparison of angle measurement

We also selected 100 X-ray images of stable bony rings as testing data for angles calculate. Figure 12 shows the angle detected after mask extraction by model, which is compared with the result obtained by image processing software after the hipbones centerline's manual judgment. Relative error range is-5.77%~ 6.12%. According to the histogram of angle data presented in Figure 13, the angles we obtained present normal distribution. Table. 3 lists the result of the normal distribution test. In the Shapiro Wilk test and Kolmogorov Smirnov test, P values are 0.138 and 0.814, respectively. At the test level of $\alpha = 0.05$, $P > 0.05$. The original hypothesis is not rejected, and the data can be considered as the normal distribution. After removing abnormal data using the z-score and normal distribution characteristic, the final angle range is 42° ~ 65°.

Table 3: Comparison of angle measurement

			Statistic
Angle between hipbones	Mean		53.28
	95% Confidence Interval for Mean	Upper Bound	52.03
			54.53
	5% Trimmed Mean		53.30
	Median		54.00
	Variance		39.375
	Std. Deviation		6.275
	Skewness		-0.077
	Kurtosis		0.251
Kolmogorov-Smirnov[a]	Statistic		0.078
	df		100
	Sig.		0.138

Shapiro-Wilk	Statistic	0.992
	df	100
	Sig.	0.814

a. Lilliefors Significance Correction

DISCUSSION

Pelvis plays an essential role in human bones. When the pelvic fractures, the tissues and organs in the pelvis and the ligaments attached to the bone surface may be damaged, they are leading to complications, such as hemorrhage associated with a high mortality rate. Commonly, severe pelvic trauma mainly due to vehicle crashes or falls from significant high. Rapidly diagnosing is most critical for survival and reduction of morbidity. Surgeons usually use X-rays to detect fractures, especially in poor medical conditions of the characteristics, low radiation, simple operation, and cost-effectiveness. Therefore, x-ray image segmentation has attracted considerable attention.

In the present research, we used the data collected from the open-source medical database to retrain the model of Mask R-CNN, a method for detecting and segmenting objects in images that extends Faster-RCNN. Then, the retained model's masks are used to detect ramus fracture by testing the obturator's integrity foramen and generating the center lines of hipbones. Finally, we calculate the range of angle between hipbones to provide a basis for judging whether unstable bones occur, and we obtained a favorable result.

D.J Withey et al. classified medical image recognitions and segmentation methods into three generations [10]. The first generation adopted the basic computer image processing techniques, such as Thresholds, Region Growing, and edge tracing [11], which uses the processing of image pixels to obtain the region of interest. The first generation's main limitation is that prior knowledge is ignored, and the results are highly susceptible to image quality. In the second-generation segmentation method, the uncertainty model and optimization methods are introduced. For example, Xueqin Li et al. use the maximum fuzzy entropy to determine the threshold method in breast cancer detection [12]. The third generation combines a priori information and a deformable model to improve the accuracy of recognition. Deformable models include Shape Models, Appearance Models, and so on [13]. The disadvantage of these two methods is convergence, including speed and accuracy, depends on the initial shape. If the initial shape is far from the actual shape, not only will the number of iterations increase significantly, but the likelihood of convergence to local minima increases [14]. With the rapid development of deep learning, neural networks have been increasingly applied to the segmentation of medical images, such as liver lesion classification, Chest pathology detection, and Brain tumor segmentation, etc. [26, 27, 28]. However, there is no method for adapting the convolutional neural network to automatic pelvis segmentation.

In our research, some significant deviation results in the angle detection results, some of which are more than 6%. The current segmentation accuracy is limited by the number of images in the training dataset, increasing the amount of data can help improve the segmentation effect. In addition, the range of hip bone angles was calculated from the unclassified dataset and no information such as age, gender, etc. was added during the model training. The method proposed in this paper is merely to verify the feasibility of the method in hip bones clamping angle measurement and identification of anterior pubic fractures so that subsequent studies can further classify pelvic fractures for patients of different sexes and ages on this basis.

CONCLUSION AND FUTURE WORK

In this paper, we retrained the model of Mask R-CNN, which was designed for image segmentation to detect superior ramus fractures. Besides, we provide an angle basis for judging pelvic stability when surgeons evaluate the mechanism of injury.The method we proposed is to segment hip bones and obturator foramen in X-ray films, which is a simple and economical detection technology; therefore, this method is more helpful for some areas with poor medical conditions. Future work will focus on establishing a database with higher quality and classified according to Mechanisms of injury to improve the segmentation effect and reduce the angle detection error.

ACKNOWLEDGMENT

Authors would like to thank Prof. Oe, for providing medical advice.

REFERENCES

1. Cordts Filho R M, Parreira J G, Perlingeiro J A G, et al. Pelvic fractures as a marker of injury severity in trauma patients[J]. Revista do Colégio Brasileiro de Cirurgiões, 2011, 38(5): 310-316.
2. Lewallen LW, McIntosh AL, Sems SA. Pediatric Pelvic Ring Injuries. Orthopedics. 2018 Sep 01;41(5):e701-e704.
3. Barratt RC, Bernard J, Mundy AR, Greenwell TJ. Pelvic fracture urethral injury in males-mechanisms of injury, management options and outcomes. Transl Androl Urol. 2018 Mar;7(Suppl 1):S29-S62
4. Platz A, Heinzelmann M, Trentz O. (i) Assessment principles and management of major trauma beyond ATLS®[J]. Current Orthopaedics, 2001, 15(3): 167-175.
5. Holstein J H, Culemann U, Pohlemann T, et al. What are predictors of mortality in patients with pelvic fractures?[J]. Clinical Orthopaedics and Related Research®, 2012, 470(8): 2090-2097

6. Demetriades D, Karaiskakis M, Toutouzas K, et al. Pelvic fractures: epidemiology and predictors of associated abdominal injuries and outcomes [J]. Journal of the American College of Surgeons, 2002, 195(1): 1-10.
7. Mettler Jr F A, Huda W, Yoshizumi T T, et al. Effective doses in radiology and diagnostic nuclear medicine: a catalog[J]. Radiology, 2008, 248(1): 254-263.
8. Obaid A K, Barleben A, Porral D, et al. Utility of plain film pelvic radiographs in blunt trauma patients in the emergency department [J]. The American Surgeon, 2006, 72(10): 951-954.
9. Lunsjo K, Tadros A M A, Hauggaard A, et al. Acute plain anterioposterior radiograph of the pelvis is not useful in detecting fractures of iliac wing and os sacrum: a prospective study of 73 patients using CT as gold standard[J]. Australasian radiology, 2007, 51(2): 147-149.
10. Withey, Daniel J. and Zoltan J. Koles. "A Review of Medical Image Segmentation: Methods and Available Software." (2008).
11. Sklansky J. (1976) Boundary Detection in Medical Radiographs. In: Preston K., Onoe M. (eds) Digital Processing of Biomedical Images. Springer, Boston, MA
12. Li X, Zhao Z, Cheng H D. Fuzzy entropy threshold approach to breast cancer detection[J]. Information Sciences-Applications, 1995, 4(1): 49-5
13. Cootes T F, Taylor C J. Statistical models of appearance for medical image analysis and computer vision[C]//Medical Imaging 2001: Image Processing. International Society for Optics and Photonics, 2001, 4322: 236-248.
14. Zhao S, Gao W, Shan S, et al. Enhance the alignment accuracy of active shape models using elastic graph matching[C]//International Conference on Biometric Authentication. Springer, Berlin, Heidelberg, 2004: 52-58.
15. The National Library of Medicine presents MedPix. https://medpix.nlm.nih.gov/home, Accessed 25 February 2021.
16. [16] DICOM library, https://www.dicomlibrary.com/, Accessed 25 February 2021.
17. A. Setio et al., "Pulmonary nodule detection in CT images using multiview convolutional networks," IEEE Trans. Med. Imag., vol. 35, no. 5, pp. 1160–1169, May 2016.
18. Pratt H, Coenen F, Broadbent D M, et al. Convolutional neural networks for diabetic retinopathy[J]. Procedia Computer Science, 2016, 90: 200-205.
19. Prasoon A, Petersen K, Igel C, et al. Deep feature learning for knee cartilage segmentation using a triplanar convolutional neural network[C]//International conference on medical image computing and computer-assisted intervention. Springer, Berlin, Heidelberg, 2013: 246-253.

20. Alton, Timothy B., and Albert O. Gee. "Classifications in brief: Young and Burgess classification of pelvic ring injuries." (2014): 2338-2342.
21. Dalal S A, Burgess A R, Siegel J H, et al. Pelvic fracture in multiple trauma: classification by mechanism is key to pattern of organ injury, resuscitative requirements, and outcome[J]. The Journal of trauma, 1989, 29(7): 981-1000; discussion 1000-2.
22. He K, Gkioxari G, Dollár P, et al. Mask r-cnn[C]//Proceedings of the IEEE international conference on computer vision. 2017: 2961-2969.
23. T.-Y. Lin, M. Maire, S. Belongie, J. Hays, P. Perona, D. Ramanan, P. Dollar, and C. L. Zitnick. Microsoft COCO: Common objects in ´ context. In ECCV, 2014.
24. Ketaro Wada, labelme: Image Polygonal Annotation with Python,2016; software available at https://github.com/wkentaro/labelme.
25. Lin, Tsung-Yi, et al. "Feature pyramid networks for object detection." Proceedings of the IEEE conference on computer vision and pattern recognition. 2017.
26. Frid-Adar M, Diamant I, Klang E, et al. GAN-based synthetic medical image augmentation for increased CNN performance in liver lesion classification[J]. Neurocomputing, 2018, 321: 321-331.
27. Bar Y, Diamant I, Wolf L, et al. Chest pathology detection using deep learning with non-medical training[C]//2015 IEEE 12th International Symposium on Biomedical Imaging (ISBI). IEEE, 2015: 294-297.
28. S. Pereira, A. Pinto, V. Alves, and C. A. Silva, “Brain tumor segmentation using convolutional neural networks in MRI images,” IEEE Transactions on Medical Imaging, vol. 35, no. 5, pp. 1240–1251, 2016.